HiSST: 3rd International Conference on
High-Speed Vehicle Science Technology

14–19 April 2024, Busan, Korea

Aerothermal Loads Analysis of ReFEx by coupled CFD Calculations

M. Franze[1], V. Wartemann, C. Merrem, H. Elsäßer[2], T. Ruhe, T. Eggers, H. Weihs

Abstract

The Reusability Flight Experiment (ReFEx) is an experimental vehicle, which is developed by the German Aerospace Center (DLR). It simulates the re-entry of a reusable booster stage. After being propelled with a VSB30 rocket to an altitude of about 135 km it will perform an autonomous re-entry. This paper is focused on the analysis of the aerothermal loads. Different approaches are applied for the investigations of the thermal heating: from a very conservative worst-case analysis up to a full-coupled simulation via the DLR $CoNF^2aS^2$ tool (Coupled Numerical Fluid Flight Mechanic And Structure Simulation). The trajectory includes the launch as well as re-entry flight phase. The focus of the heating process analysis is on the experimental ReFEx vehicle itself.

Keywords: *Reusability Flight Experiment ReFEx, reusable booster, $CONF^2AS^2$, coupled CFD simulation, aerothermal loads*

Nomenclature

Abbreviations

CFD	Computational fluid dynamics
$CoNF^2aS^2$	Coupled Numerical Fluid Flight Mechanic And Structure Simulation
DB	Dataset Based
DLR	German Aerospace Center
EI	Entry Interface
EoE	End of Experiment
FFTB	Flux Forward Temperature Back
FSI	Fluid-Structure-Interaction
HF	Heatflux
KTR	Koonibba Test Range
MORABA	Mobile Raketenbasis (Mobile Rocket Base) of the DLR
MoS	Margin of Safety
ReFEx	Reusability Flight Experiment
RLV	Reusable Launch Vehicle
VSB30	Veículo de Sondagem Booster30 (Booster Sounding Vehicle)
TFFB	Temperature Forward Flux Back
TPS	Thermal Protection System

Latin

h	Altitude
M	Mach number
p	Pressure
$\dot{q}$	Heatflux
T	Temperature
t	Time

Greek

ρ	Density
Ω	Coupling Domain

Superscripts

f	Fluid
s	Structure

Subscripts

LE	Leading Edge
n	Number of timesteps
ref	Reference Values

1. Introduction

The hypersonic flight experiment ReFEx has been developed by the German Aerospace Center (DLR) since 2018 and is currently in the final integration status. ReFEx has a mass of around 400 kg, a length of

[1] *German Aerospace Center (DLR), Spacecraft Department, Institute of Aerodynamics and Flow Technology, Braunschweig, Germany, Marius.Franze@dlr.de, Viola.Wartemann@dlr.de, Clemens.Merrem@dlr.de, Thino.Eggers@dlr.de*

[2] *German Aerospace Center (DLR), Space System Integration Department, Institute of Structures and Design, Stuttgart, Germany, Henning.Elsaesser@dlr.de, Tobias.Ruhe@dlr.de, Hendrik.Weihs@dlr.de*

2.7 m and deployable wings with a span of 1.1 m. It will be launched on a VSB-30 sounding rocket from the Koonibba Test Range (KTR) in southern Australia in 2024, reaching velocities of up to Mach 5 and an altitude of around 135 km on a suborbital trajectory. The planned trajectory is representative of an aerodynamically controlled RLV-booster stage, where ReFEx will test several key technologies required for future reusable aerodynamically controlled first stages, see Rickmers et al. [14].

The following requirements are some of the main drivers of the ReFEx design Bauer et al. [3]:

- The vehicle shall perform an autonomously controlled flight from hypersonic to subsonic velocities to a predefined point in space (latitude, longitude, altitude) with a predefined terminal velocity, following the typical Mach-profile as a function of altitude of an aerodynamically controlled stage
- The vehicle shall perform a controlled heading change. The angle between a line connecting the apogee and the entry interface (EI) and a line connecting the EI and end of experiment (EoE) shall exceed 30°
- Reach a prescribed target point (EoE) within a certain accuracy (altitude, velocity and geographic position)

The key mission events and timeline can be seen in figure 1: ReFEx is launched on a VSB-30 sounding rocket, consisting of the S31 first stage and the S30 second stage provided by MORABA. Just after burn-out of the second stage the vehicle is de-spun using a yoyo-system, the fairings are separated and its actual experimental mission begins. Once in free flight, ReFEx unfold its wings, which were stored underneath the fairing. In figure 2 ReFEx including the S31 and S30 motors as well as split fairing in lift-off configuration is illustrated. Back to figure 1: The experimental phase starts outside of any notable atmospheric influence. Hence ReFEx uses a small reaction control system to orientate itself into an aerodynamically stable state to enter the aerodynamically dominated part of the re-entry without any difficulty. The initial deceleration is done at high angles of attack to keep the structural and aerothermal loads within an acceptable range. The orientation counterintuitively is a belly-up position. The main reason here is stability along the longitudinal roll axis. Once ReFEx reaches the lower regions of the

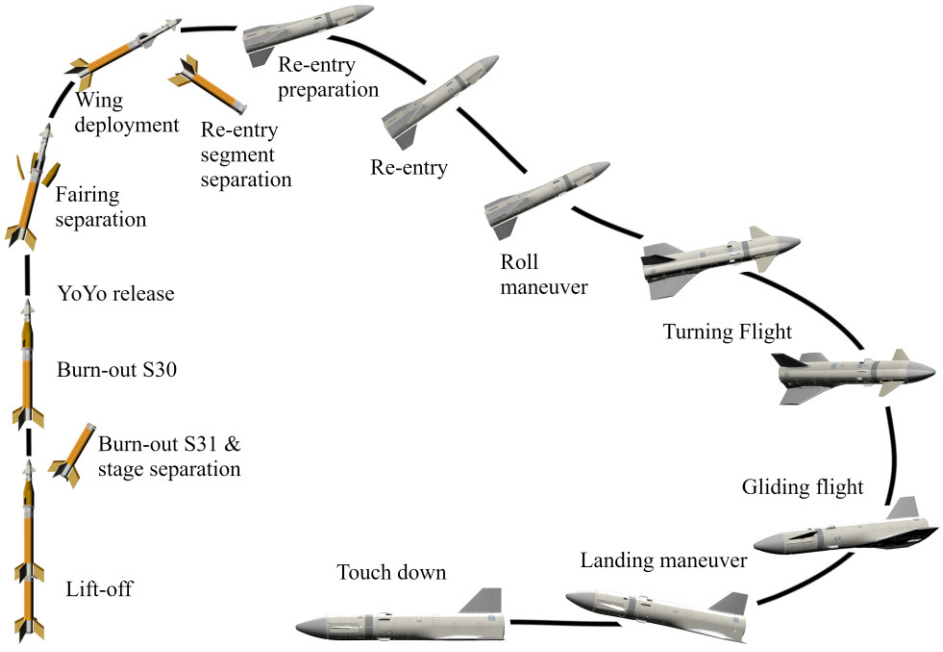

Fig 1. Mission overview and key flight maneuver.

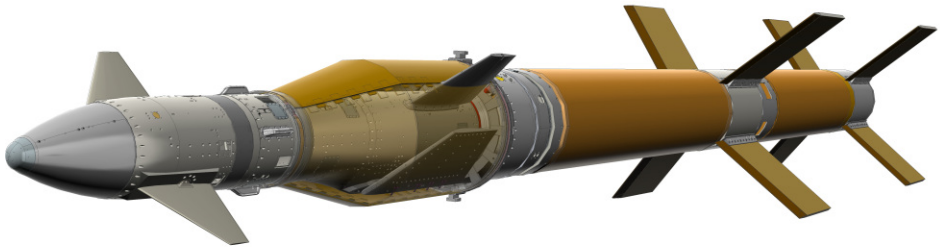

Fig 2. CAD model of ReFEx incl. S31 and S30 motors as well as split fairing in lift-off configuration.

atmosphere (approximately at Mach 1.5) it performs a roll maneuver to the belly-down position. In this flight phase the angle of attack is decreased to fly at angles close to a state of the maximum lift-to-drag ratio, which is around an angle of attack of 10° and continue the flight to EoE. After reaching EoE the main mission for ReFEx is complete, since automated landings in subsonic flight are well demonstrated. However, in an effort to preserve the integrity of the in-flight data recorders for the belly landing (a landing gear was outside of the scope of the project), the flight is continued to be guided. The goal here is to minimize impact energy and avoid certain no-go areas, where the vehicle could be very difficult to recover. [14, 3]

One key technology for a RLV is the Thermal Protection System (TPS). A major prerequisite for choosing and layout a TPS is the quantification of thermal loads. In this paper, different approaches are applied for the investigation of the aerothermal heating: from a very conservative worst-case analysis up to a full-coupled simulation via the DLR $CoNF^2aS^2$ toolchain. The trajectory includes the launch and re-entry phase. The focus of the aerothermal heating process analysis is on the experimental ReFEx vehicle itself.

2. Analysis of aerothermal loads

Different approaches can be used for the analyses of thermal heating from low- to high-fidelity, depending on the available time, the computer capacities and the requested/needed accuracy of the results. In this chapter different methods, which were applied during the layout process and for further ongoing analyses, are outlined.

The regular DLR development process follows in general the classical V-model of systems engineering to analyze a first design space and achieve possible solutions. Due to the complex ReFEx mission requirements a lot of variables had to be considered at the beginning (e.g. trajectories, sizing, launcher systems, etc.). To handle this early in the project (pre-phase/phase A) in an economic way, an additional agile design loop was introduced into the V-model by developing an extended dataset based thermo-mechanic analysis, compared to standard pre-methods (see chapter 2.1 and 2.2)). To predict precise temperatures for the whole vehicle, full-coupled unsteady simulations are required, see chapter 2.3. For this unsteady simulation with $CoNF^2aS^2$, DLR TAU calculations for CFD along the whole trajectory are performed, considering the material properties through coupling using a high fidelity structural model. The different methods will be analyzed and evaluated.

The reference flight trajectory is given is figure 3. For the investigations in this paper, which are focused on the heating process, the trajectory of the complete ascent and the re-entry flight phase up to a flight point near the roll maneuver is considered. Due to change of the vehicle orientation from belly-up to belly-down, the critical/highest wall temperatures will be approached before the roll maneuver itself. Thus the last part of the trajectory after the roll maneuver can be neglected. The figure depicts the altitude h, Mach number M and angle of attack (α, AoA). Additionally, the selected flight points for the comparison in chapter 2.2 and 2.3 are illustrated as squares. The circled flight points along the altitude curve are used during the pre-analyses in the following chapter.

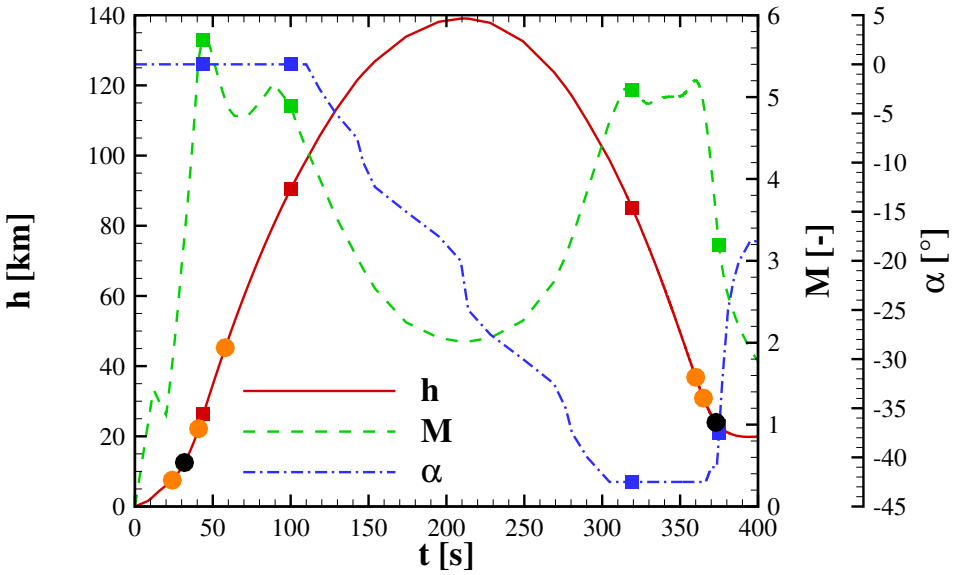

Fig 3. Flight trajectory and selected flight points for data comparison.

2.1. Fast pre-analyses for the layout

Different fast, especially low-fidelity, methods exist for the pre-analysis of the wall temperature/heat flux. For example, the DLR HOTSOSE code [13], which is a low-fidelity aerodynamic and aerothermodynamic design tool, can be used for the evalution of the aerodynamic heating by different methods. These methods depend on the vehicle geometry. The stagnation point can be calculated by the formulations of Fay-Riddell [4] and Zody, Moss and Sutton. The heating of vehicle with blunt leading edges can be considered by the Fleming and Krauss method. Furthermore, the reference enthalpy method and the White-Christoph formulation can be applied to flat plates. A detailed comparison of different fidelity approaches for the coupled aerothermodynamic heating of hypersonic re-entry vehicles can be found in reference [2].

One other method for a simple worst-case pre-analysis of the aerothermodynamic loads can be the analysis of one selected flight point, where the maximal wall temperature occurs. Due to the already existing CFD meshes at this point of the vehicle layout, that was a fast method to receive a first impression of the maximal worst-case surface temperatures. This calculation is exemplary shown in figure 4, which is performed with the DLR CFD solver TAU (the detailed description of the DLR TAU code is given in section 2.3.3). For the investigated trajectory the flight point with the maximal heat flux density $\dot{q}_{\max}$ of the re-entry trajectory is at a Mach number of 4.9 and an angle of attack (AoA) of −42.5°. For the worst-case scenario, a radiative equilibrium boundary condition is applied. The result is visible in figure 4, which shows the worst-case wall temperature with a maximum of around 1200 K (∼930°C). Due to the short flight time the real temperature will be lower.

After this first adiabatic computation, resulting in a high conservative deviation, a preliminary material choice was made. In a second step this is evaluated with a simplified transient analysis of the full 3D ReFEx pre-structure model. For this a 3D heat flux calculated in DLR Tau Code for cold wall condition is performed for two dedicated flight points: first during up-leg (0°AoA), and second for the first critical phase during re-entry (-42.5°AoA). Those are scaled due to normalized transient-stagnation-point-heat-flux by Fay-Riddell [4] over the respective flightpath. This allows among others to evaluate different ReFEx trajectories in an efficient way, e.g. regarding lower flight paths, longer flight duration, different vehicle configurations etc.

Figure 5 shows the peak heated time point at $t = 77.9$ s. Unfortunatelly, the design space would be hardly

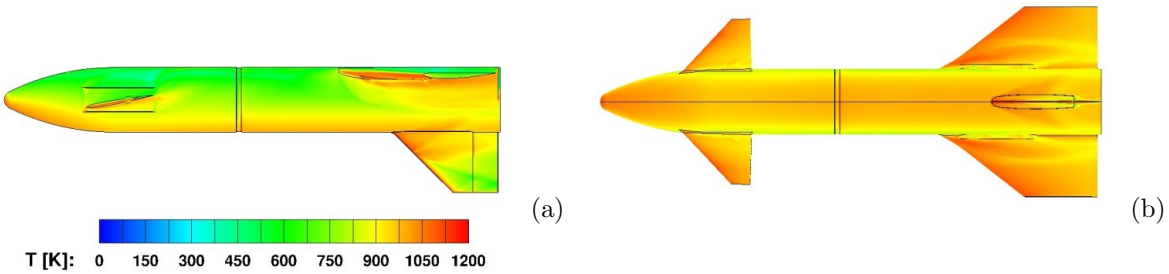

Fig 4. Temperature – distribution of $\dot{q}_{max}$ flight point (re-entry).

reduced, because the canards reach values above 1600 K and the main fuselage above 600 K.

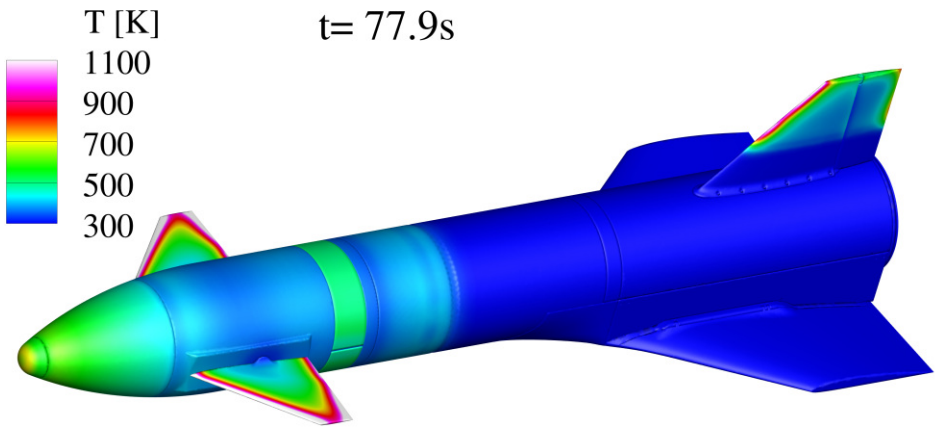

Fig 5. Peak heating at $t = 77.9$ s from conservative approach.

Due to the cold wall assumption for heat flux calculation this is still a conservative analysis, with known rising deviation especially at hotter structures.

2.2. File exchange based CFD/structure coupling

Therefor a third analysis was developed, in this case a more detailed and extended dataset based analysis by using the outcome of the second iteration, based on an almost fixed ReFEx reference trajectory. For this third analysis four flight points at up-leg and four flight points along the re-entry phases where defined. Figure 3 depicts these further supporting flight points calculated in DLR TAU code along the trajectory with the *black* and *orange* circles.

To improve accuracy, each 3d heat flux at these flight points is computed for dedicated uniform body temperatures in an automated process, standalone just in DLR TAU code. As the structural design is still varying in this phase, independency within the work processes between the involved DLR departments is given as a big advantage, regarding DLR TAU code heat flux calculations and the thermomechanical design. The TAU code dataset is used in ANSYS FEA to make final adaptions and verify the design at this status. The temperatures at the reference points for this third analysis are depicted and compared with the full coupled method in figures 11 and 12.

The final ReFEx design is based on the third analysis. The average thermal load of the titanium canards reaches approx. 820 K, the aluminium main fuselage is calculated to approx. 470 K. To gather some Margin of Safety (MoS), both structure units are protected with a ceramic coating to reduce the max. temperature, additionally. Furthermore, these results were used to estimate the overall thermal bending of the vehicle along the flightpath and estimate its influence in aerodynamic values for flight control, which is summarized in [10].

The calculated local thermal overload of the outer canard structures is driven by the vehicle nose shock interference. Due to the few supporting points the shock is, unlike in reality, quasistatic on that dedicated part of the canard-structure at the calculated DLR TAU code supporting points. This kind of interference and regions with high thermal gradients are represented with limited accuracy within this method and lead to more conservative local results. These regions have to be crosschecked with further analysis.

2.3. Loose coupled unsteady FSI simulation

2.3.1. Numerical Methods

This section of the paper presents a fully coupled CFD solver DLR TAU in a loose scheme with the CSM solver ANSYS FEA. It is implemented withing the $CoNF^2aS^2$ process chain, which builds on top of the FlowSimulator [12, 9]. The data exchange is realised withing the RAM of the computer to reduce IO time and written and read files, which can slow down this kind of computation, depending on the size of the problems.

The starting point of the unsteady FSI calculation for the upleg simulation is at $t = 0\,\mathrm{s}$ at an altitude of 0 km. For the downleg, start of the simulation is at $t = 319.3\,\mathrm{s}$ at an altitude of 85 km where the laws of continuum flow are valid. At higher altitude the Knudsen number would be bigger than 0.01 at the border to rarefied gases where slip flow effects start to evolve at such low densities that the molecular mean free path is not negligible.

Depending on the calculated altitude along the flight path the ICAO [11] atmosphere is used as atmospheric conditions and set at each calculated time step.

The flight parameters regarding the given trajectory parameters position, velocity, rotational rates and angles of attack, is applied by a forced motion on the CFD mesh. The inflow condition is set to zero, but the mesh itself moves with the given motion in space. In this work no flight mechanic solution is involved although $CoNF^2aS^2$ is capable to do so.

The solvers used in this paper are the DLR TAU code for the fluid domain and the commercially available suite ANSYS FEA Mechanical in version 2022R2 [1] for the structure domain. The calculated time steps are $\Delta t = 0.1\,\mathrm{s}$.

2.3.2. Coupling of Solvers

The load transfer is realized by marker based interpolations from the CFD interface mesh to the CSM interface mesh and vice versa. In this paper every surface points of the outer shells of each mesh will be used for interface meshes. $CoNF^2aS^2$ is capable of a pure deformation and thermal analysis simulation in steady and unsteady cases as well as combined solutions where deformations and thermal heating gets calculated in one single run.

For an aerothermal analysis, two different schemes are available. The CFD solver either sends heatflux to the CSM solver and gets surface temperatures back ($FFTB$ - *Flux Forward Temperature Back*) or the resulting surface temperature from the CFD calculation gets interpolated on the CSM mesh, which gives the heatflux back ($TFFB$ - *Temperature Forward Flux Back*). Depending on the problem one or the other method is more numerically stable. In this work the $FFTB$ scheme for the transient thermal only analysis is used.

Figure 6 shows the loose coupling scheme of the partitioned single domain solver for CFD and CSM. At the first coupling step, a steady fluid solution is generated at $t = 0\,\mathrm{s}$. Then the initial conditions gets exchanged at coupling step 1.0 and the CSM solver calculates the heating inside the body. Then the newly generated surface temperature gets interpolated on the CFD mesh and a new heatflux gets calculated towards the new time step t_{n+1} resulting in the first predictor step. Depending on the amount of coupling subcycles, this looping procedure can be run through several times reaching an abort criteria, after which the next time step gets calculated and so on. Depending on the altitude and velocity of the flight path the coupling procedure needs about 3 to 10 inner cycles to reach its abort criteria. If the heatflux gets bigger at higher speeds and denser atmospheres the process usually needs more inner cycles to converge.

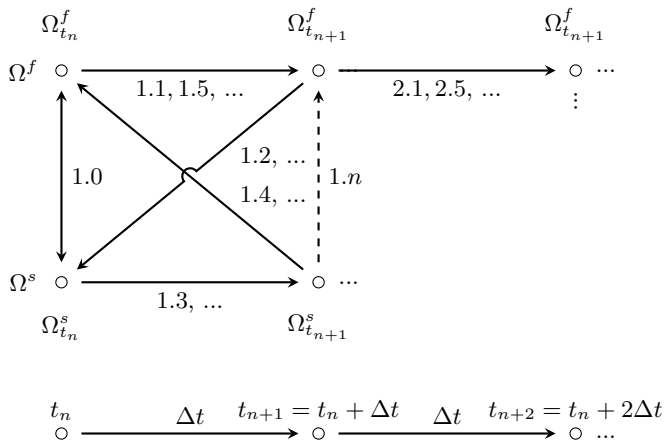

Fig 6. Loose partitioned Fluid-Structure-Interaction (FSI) coupling scheme of the single domain solver for fluid Ω^f and structure Ω^s.

2.3.3. DLR TAU code - Fluid domain

DLR TAU is a three-dimensional parallel hybrid multigrid code and has been validated for subsonic, transonic and hypersonic flows (shown in, e.g.: Schwamborn et al. [16], Langer et al. [7] or Mack et al. [8]). It solves the Reynolds-Averaged Navier-Stokes (RANS) equations using a second-order finite-volume method and is adapted for large scale simulations on high performance cluster (HPC) systems. The efficiency of the code makes it widely used in industrial as well as scientific applications for steady and unsteady flow phenomena and whole air- and spacecraft configurations. Under the variety of available turbulence models the Spalar-Allmaras one equation model in its negative formulation is used [17]. This model has already proven to be robust and sufficient for high speed vehicles [15].

An AUSMDV flux vector splitting upwind scheme [18] has been used along the whole flight trajectory. To minimize possible uncertainties regarding laminar turbulent boundary layer transition the surfaces of ReFEx are modeled as fully turbulent.

As thermodynamic model within DLR TAU an equilibrium (EQ) as well as a non-equilibrium gas model (NEQ) is used, both in thermal equilibrium. The equilibrium model uses 11 gas species because it can be computed much faster where the non-equilibrium model only contains 5 species, because each add an energy equation to be solved during runtime as Gupta [6] presents, all shown in table 1. For the EQ model a gas mixture database can be generated a priori using Polynomials provided by Gordon [5], which saves computational time during the solution process. Each model set a mass fraction of 76 % N_2 an 24 % O_2 as inflow condition. The production of the residual species get calculated during the calculation according to local mixture rules depending on pressure, density and gas composition.

Table 1. Used thermodynamic gas models and calculated species.

Model	Number of Species	Species
EQ	11	N_2, O_2, NO, N, O, N_2^+, O_2^+, NO^+, N^+, O^+, e^-
NEQ	5	N_2, O_2, NO, N, O

As the velocities and altitudes on the upleg computation are moderate, the faster EQ model is used for this segment. The computationally more challenging NEQ model is applied for the downleg, because the much higher velocity and altitude at the beginning of the reentry can cause realgas effects at much higher gas temperatures, compared to the first half of the trajectory.

The dimensionless value y^+ changes significantly over flight time and velocity. At the beginning at low mach numbers it is just under 3.5 on the main surface areas, reaching values below 1.0 and well under

0.1 for the major part of the trajectory, which are most relevant for the aerothermal loads, as table 2 shows.

Table 2. y^+ along flight time.

Time	0 s – 10 s	20 s	30 s	35 s	40 s	50 s	350 s	375 s
y^+	<3.5	<2.0	<1.5	<1.0	<0.5	<<0.1	<0.1 s	<1.0

Figure 7 shows the hybrid mesh of the fluid domain. The field mesh contains 45.0 M nodes, whereas the surface alone consists of 1.0 M points. Especially the volume mesh is rather fine resolved, which is necessary to get a smooth resolution of the developing inclining shock during flight and a smooth temperature distribution on the surface. The mesh adaptation feature within DLR TAU was not applied, because it would have been necessary to run it after every timestep, which makes it more time consuming than computing the shown finer mesh in the near farfield.

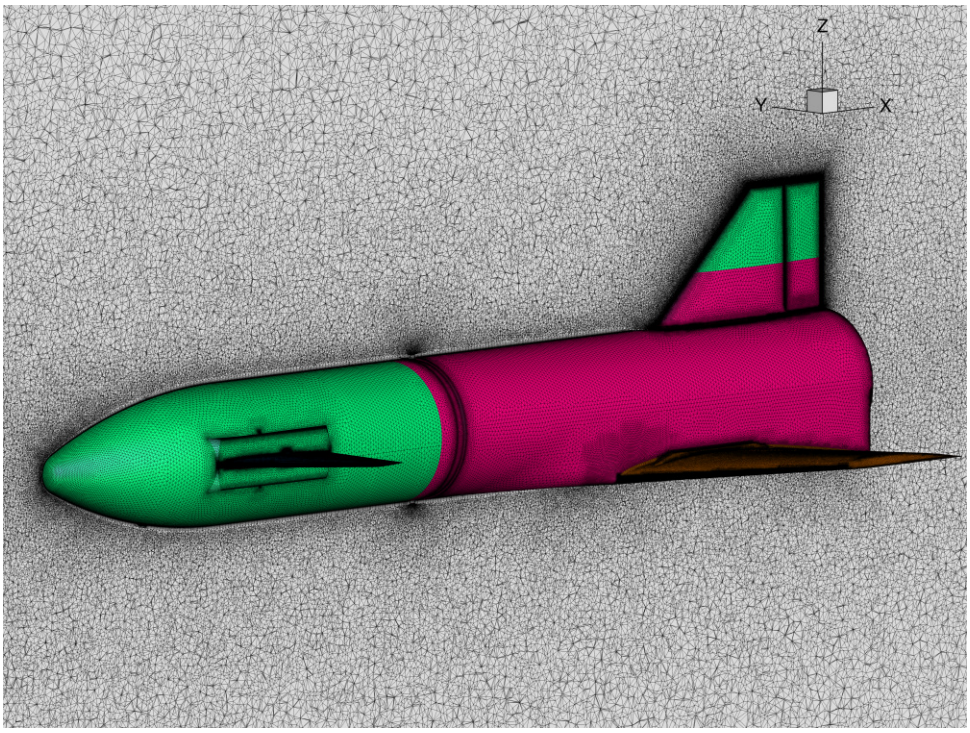

Fig 7. CFD surface mesh and $y = 0$ slice.

2.3.4. Ansys - Structure domain

As high fidelity structural solver the commercially available suite called *ANSYS Mechanical 2022 R2* is applied by means of a 3D transient thermal analysis sparse solution. It gets the heatflux from the fluid domain, calculates the structural heating and gives the resulting surface temperatures back.

Figure 8 shows the surface mesh, which again, is rather fine resolved to get smooth transitions along the bodies. Within the CSM solver, quadratic tetrahedra elements are used for each of the parts. The structural model itself is the same between the discussed coupling methods. It consists of 56 bodies with varying materials, which are connected with contact elements, transferring the loads between them in both directions.

The total number of grid points equal to 5.8 M nodes for the volume mesh alone and 0.17 M points for the interface mesh for the upleg (*green*) and 1.1 M points for the interface mesh for the downleg simulation (*red* and *green*).

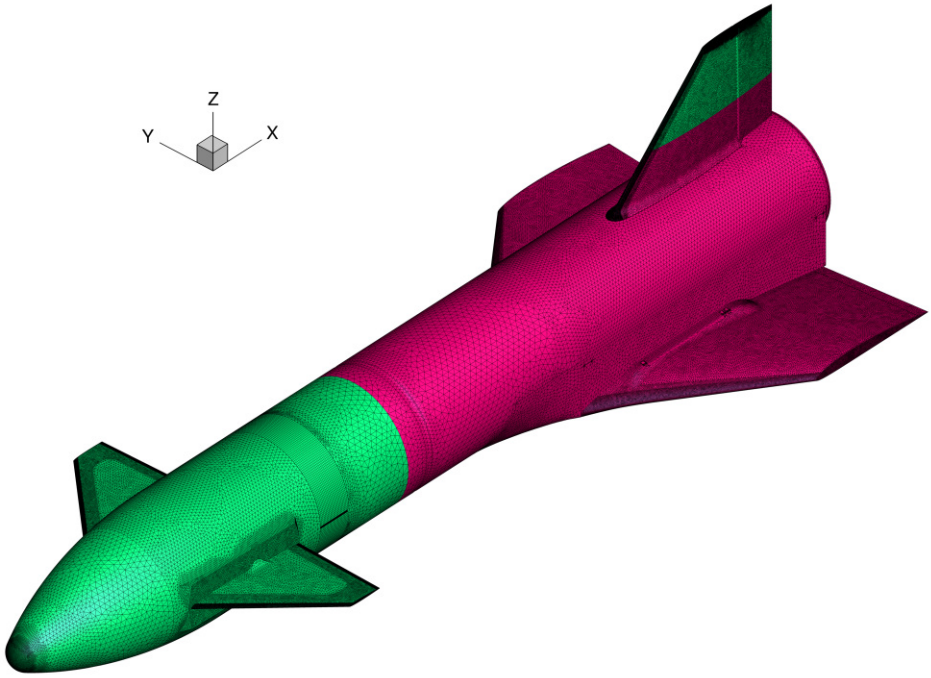

Fig 8. CSM surface mesh.

During the upleg flight the region of the *red* interface, for both CFD and CSM mesh, is hidden under the split fairing as figure 2 displays. For this reason is is inactivated during the upleg simulation as well and added as an additional interface mesh when the reentry simulation starts, after the fairing separated and exposed the surfaces to the surrounding flow as figure 1 shows.

Similarly the connected S30/S31 motor combination is present in the real flight condition during the upleg, but is not modelled in the simulation, because their aerothermal performance or influence on the ReFEx payload was not a scope of this work.

2.4. General Flow Phenomena Description

This chapter describes the general flow phenomena along the calculated trajectory to explain the selection of the flight points used for method comparison in chapter 2.5 and planting the fundamentals for the temporal evolution of the temperature cuts.

Figure 9 illustrates five selected flight point at the upleg simulation at $\Delta t = 20\,\mathrm{s}$. Each figure plots the heated surface temperature and the volume temperature in a field cut in the symmetry plane at $y = 0\,\mathrm{m}$, except figure 9(a), which shows the mach number in the field, because of the low temperatures at the beginning of the trajectory.

The simulation starts at $t = 0\,\mathrm{s}$ with a cold wall and just the *green* interface meshes in the coupling process at an altitude of $h = 0\,\mathrm{km}$ and a mach number of $M = 0$. Although the real geometry is changed during flight with the retractable wings, the meshes for CFD and CSM simulations kept the same and the fairing was not modelled. This has to be in mind during the discussion of the following upleg simulation contour plots.

At $t = 20\,\mathrm{s}$ ReFEx flies through the transsonic region with $M = 1.16$, building a complex shock interacting flow field around the canard regions. The tipping point shock starts to incline and getting stronger over time as the mach number increases to $M = 5.25$ at $t = 40\,\mathrm{s}$. This time point is near the point of the maximum canard and wrap-around antenna heating at $t = 44\,\mathrm{s}$

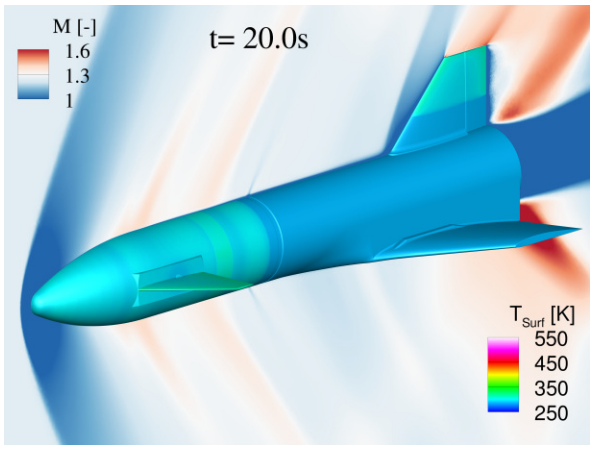

(a) $t = 20\,\mathrm{s}$.

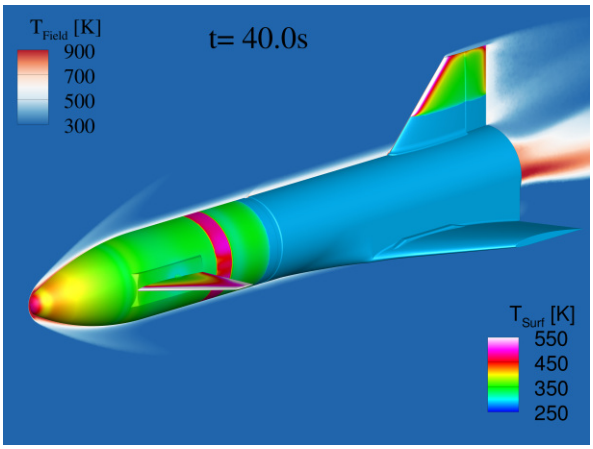

(b) $t = 40\,\mathrm{s}$.

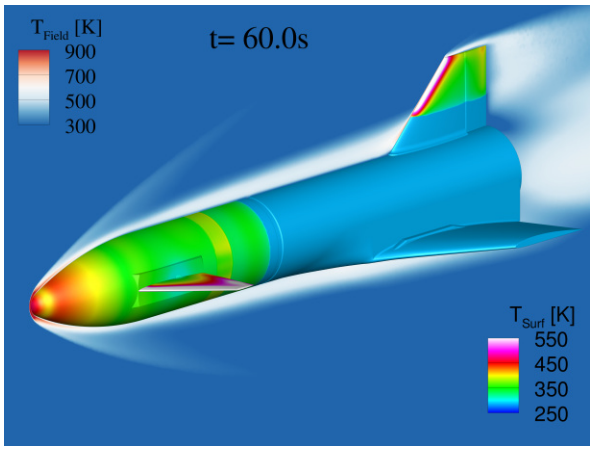

(c) $t = 60\,\mathrm{s}$.

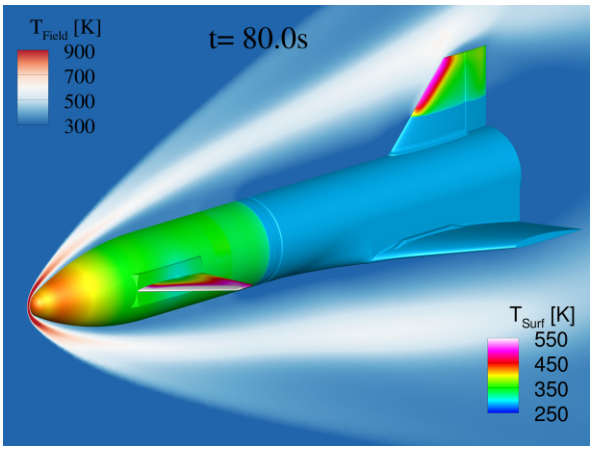

(d) $t = 80\,\mathrm{s}$.

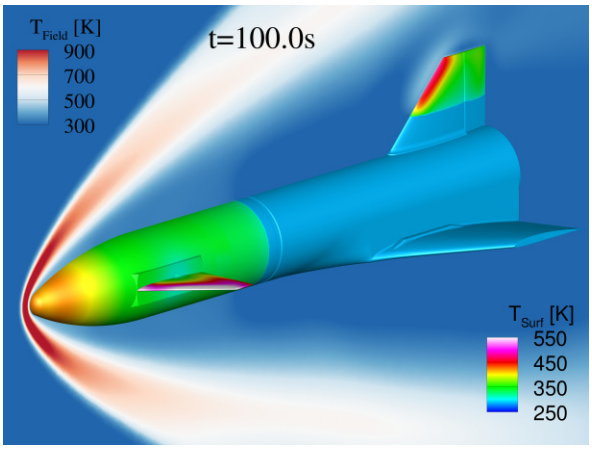

(e) $t = 100\,\mathrm{s}$.

Fig 9. Flow topology during upleg from $20\,\mathrm{s} < t < 100\,\mathrm{s}$.

In the following time steps, the shock keeps getting stronger, but the peak leading and trailing edge regions at the canards as well as side fin at the back start to cool down, because of the falling density due to raising altitude.

Beginning at $t = 80\,\mathrm{s}$ the shock starts to widen itself because of the low atmospheric pressure and density at an altitude of $h = 71.0\,\mathrm{km}$ resulting a further cooling of the structure. At $t = 100\,\mathrm{s}$ an altitude $90.4\,\mathrm{km}$ is reached, where limits of the laws of continuum flow are reached and the coupled simulation is stopped.

After $\Delta t = 219.3\,\mathrm{s}$ of radiation only CSM simulation, the reentry flight point starts at $t = 319.3\,\mathrm{s}$. Figure 10 presents two selected flight point at the downleg of the trajectory.

Unfortunately, the high fidelity coupled simulation of the upleg took more time than expected and was not finished, when the downleg simulation had to start to be in time for this work. For this reason the initial wall temperature is cold, meaning the initial atmospheric temperature at an altitude of $h = 85\,\mathrm{km}$. This can be seen in figure 10(a). Fortunately, the fairing shielded the main body and its wings during launch, which makes the fully-coupled simulation comparable to the dataset based method along these parts.

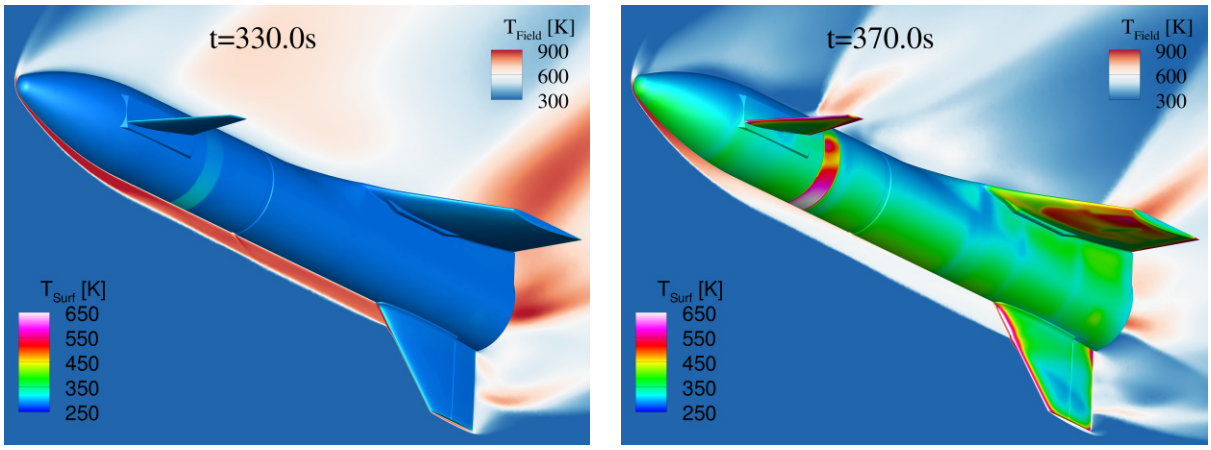

(a) $t = 330\,\mathrm{s}$. (b) $t = 370\,\mathrm{s}$.

Fig 10. Flow topology during downleg at $t = 330\,\mathrm{s}$ $t = 370\,\mathrm{s}$.

Nonetheless, figure 10(a) illustrates the huge temperature gradients occurring during reentry at the high angle of attack of $\alpha = -42.5°$ belly-up position. The fin at the back stands in the flow and the wings stabilize the vehicle like a parachute. After only $\Delta t = 40\,\mathrm{s}$ of flight, the upper surface heats much more compared to the bottom and the wrap-around antenna reaches temperature of over $660\,\mathrm{K}$.

Each colder region on the surface of the main body and its wings, is caused by an underlying structural body, e.g. flanges, ribs under the outer shell, acting as a heat sink reservoir, representing the high quality of the structural model used in this work.

2.5. Comparison of selected flight points

Finally the two selected methods from chapter 2.2 (dataset based - DB) and 2.3 (fully-coupled - FSI) are compared side by side at four selected flight points along the trajectory, which are listed in table 3.

The following figures 11 and 12 displays five y-plane cuts in $y = 0\,\mathrm{m}$ to $0.4\,\mathrm{m}$ per $\Delta y = 0.1\,\mathrm{m}$ and one z-plane cut in $z = 0.4\,\mathrm{m}$. The solid lines are from the FSI results whereas the dotted lines got extracted from the DB coupled method.

In general figure 11(a) shows at $t = 44\,\mathrm{s}$ good agreement along the x-axis of ReFEx. The stagnation point temperature is $\Delta T = 27\,\mathrm{K}$ higher predicted using FSI at a total value of $T = 524\,\mathrm{K}$. The leading

Table 3. Selected flight points for method comparison.

FP	Time	Altitude	Description
1	44.0 s	26.4 km	peak heating at upleg
2	100.0 s	90.4 km	at the end of the upleg full-coupled FSI calculation
3	319.3 s	85.0 km	at the beginning of the downleg fully-coupled FSI calculation
4	375.0 s	22.9 km	before the roll maneuver to start gliding phase

edge is predicted up until $\Delta T = 121\,\mathrm{K}$ at a total of $T = 711\,\mathrm{K}$ higher than using the DB method.

Along the nose cone, the FSI temperatures differ less than $\Delta T = 14\,\mathrm{K}$ lower at ranges between $T = 445\,\mathrm{K}$ till 330 K along flow direction. The heating of the main area of the canards differ only by a few kelvin whereas the peaks at the leading raise to $\Delta T = 130\,\mathrm{K}$ more using the DB method. A similar overshoot of $\Delta T = 413\,\mathrm{K}$ can be seen at the outermost trailing edge cut as well. Considering the FSI results, the canards reach up to 1010 K at their leading edges during the upleg.

The wrap-around antenna heating differs at worst by about $\Delta T = 22\,\mathrm{K}$ in the beginning at $x = 0.91\,\mathrm{m}$ approaching each other towards $x = 1.00\,\mathrm{m}$ at a total of $T = 467\,\mathrm{K}$, which is negligible for the design itself.

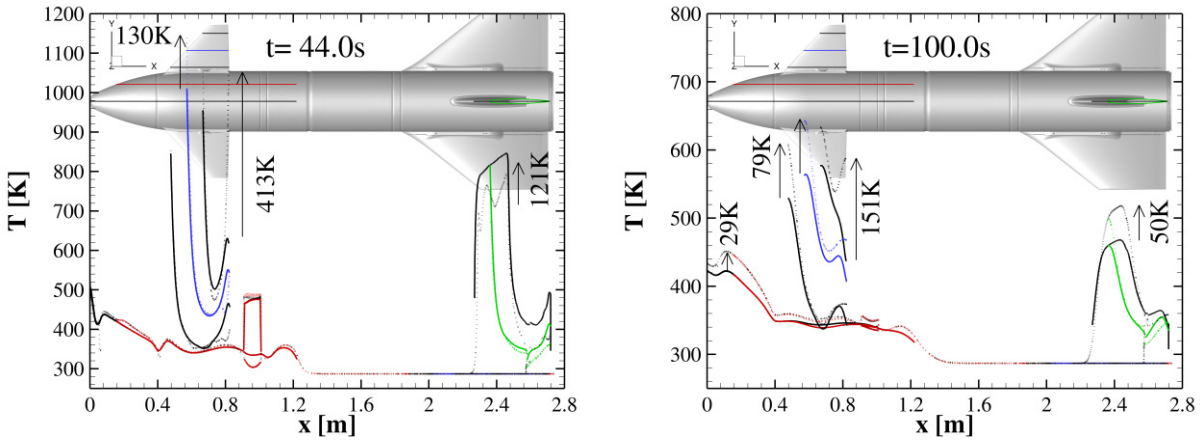

(a) $t = 44.0\,\mathrm{s}$. (b) $t = 100.0\,\mathrm{s}$.

Fig 11. Temperature distribution at $t = 44\,\mathrm{s}$ and $t = 100\,\mathrm{s}$ along five y-plane and one z-plane cuts through surfaces; *solid* - FSI; *dotted* - DB.

The differences start to gain in the following time step at $t = 100\,\mathrm{s}$ in figure 11(b). While the stagnation point temperature is $\Delta T = 10\,\mathrm{K}$ bigger the nose cone can reach up to $\Delta T = 29\,\mathrm{K}$ more at a peak of $T = 451\,\mathrm{K}$ using the DB method, which is 17% more heating from $t = 0\,\mathrm{s}$. The rest of the main body does not exceed more than $\Delta T = 11\,\mathrm{K}$ more heating until the fairing shields the second half of the vehicle. The canards main surfaces have the same difference range, which does not change by much in spanwise direction. The peaks at the leading ($\Delta T = -79\,\mathrm{K}$) and trailing ($\Delta T = -151\,\mathrm{K}$) edge on the other hand are again much smaller predicted using FSI. The maximum value reaches $T = 577\,\mathrm{K}$ at the outmost cut on the leading edge. Same applies to the fin in the back, which gets overpredicted by $\Delta T = 50\,\mathrm{K}$ at 468 K.

Compared to the former flight point, the temperatures are more distributed inside the body and the peaks are smoothed out. Especially the back fin distributed the heat from the leading edge peak at $T = 846\,\mathrm{K}$ down to 468 K.

Looking at the following time step in figure 12(a) at $t = 319.3\,\mathrm{s}$ after only radiation gets calculated, the

same applies. The peaks get smoothed more and the heat distributes over the individual parts, meaning main body, canards and fin.

The peak temperature at the nose is at 414 K for the FSI calculations and the curves of both methods near each other with gaining vehicle length as they get near the cold structure, which was under the fairing. The differences at the nose cone is less than $\Delta T = 26\,\mathrm{K}$. The canards cool down to 463 K by about $\Delta T = 114\,\mathrm{K}$ compared to the former time step. The values from the DB method are less than $\Delta T = 40\,\mathrm{K}$ higher. The fin cools further down to 386 K and additional $\Delta T = 21\,\mathrm{K}$ for the DB case respectively.

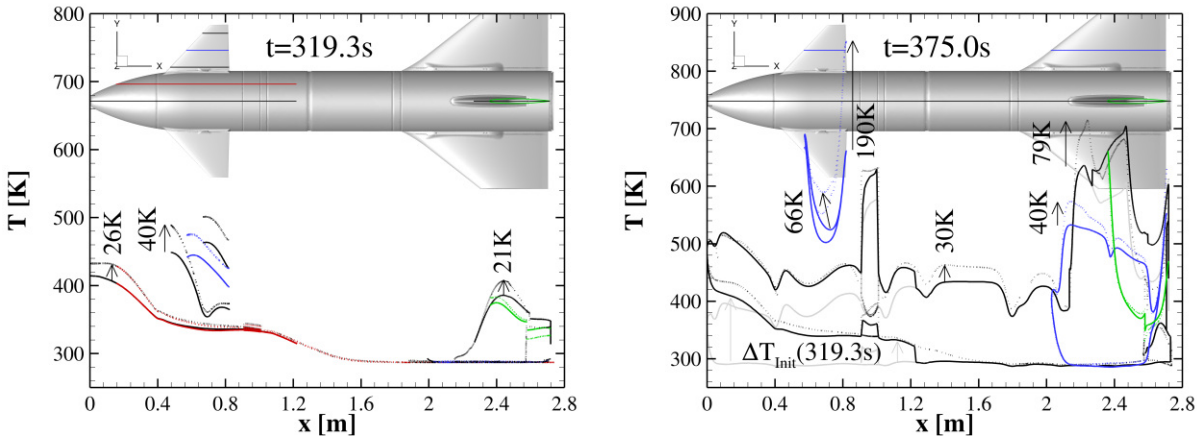

(a) $t = 319.3\,\mathrm{s}$ after $\Delta t = 219.3\,\mathrm{s}$ radiation only.

(b) $t = 375.0\,\mathrm{s}$.

Fig 12. Temperature distribution at $t = 319.3\,\mathrm{s}$ and $t = 375\,\mathrm{s}$ along five y-plane and one z-plane cuts through surfaces; *solid* - FSI; *dotted* - DB.

Entering the downleg simulation the aerothermal loads rise significantly. As stated, the downleg simulation started with a cold wall, because the upleg simulation was not finished in time. To diminish this influence on the shown data the offset temperature from the initial time point is added in post analysis and plotted in figure 12(b). Afterwards, the only difference is the slightly higher heatflux from the FSI calculation, which results from the colder initial wall.

The *grey* line in figure 12(b) shows representatively the FSI cold wall downleg result in $y = 0\,\mathrm{m}$. Adding the initial temperature to the surface yields to the *black* line.

The heated upper surface on the nose cone coincide well between the two methods, the differences are less then $\Delta T = 5\,\mathrm{K}$ at a total value between 519 K to 412 K. The wrap-around antennas peak heating of 631 K is the same, but the temperature builds a plateau in the DB calculations, where in the FSI it builds up to the peak in downstream direction. Where in most cases the DB method represents the conservative design case at this point it is in line with the FSI calculation leaving no room for safety factors.

The inner shielded surface of ReFEx at $x > 1.2\,\mathrm{m}$ reaches $T = 434\,\mathrm{K}$, which differs less than $\Delta T = 30\,\mathrm{K}$ from the DB method.

The fin heating in the lower section is $\Delta T = 79\,\mathrm{K}$ underestimated by the FSI calculation due to the initial cold wall. The upper part, on the other hand, shows $\Delta T = 23\,\mathrm{K}$ more compared to the DB method.

As was seen in the former flight points, the temperature on the canards is less in the FSI simulations. The central canard heats to about 520 K, whereas the design method predicts $\Delta T = 66\,\mathrm{K}$ more further upstream. The peaks on the trailing edge is highly overpredicted by $\Delta T = 190\,\mathrm{K}$ at 661 K for FSI.

The wing agree well to another, because they were shieldet by the faring in both cases, starting with a

cold wall at the downleg. The differences are $\Delta T = 40\,\mathrm{K}$ at $T = 533\,\mathrm{K}$ at the FSI peak heat, which is 15% more heating for the DB method.

Overall the DB method showed good agreement with the fully coupled FSI simulation. For the design process it is fast and reliable. In most areas it can be seen as the conservative approach, which is the main target of a design tool.

Time accurate FSI simulations should be used directly after the design process to assess the areas, where the conservative approach heavily underestimated the aerothermal load to be analysed to prevent failure. On the other hand in regions where the heatfluxes are lower predicted by the FSI the geometry or material combination can be optimized within the given safety margins to save weight and reduce cost.

3. Conclusion

Different approaches, from low- to high-fidelity, can be used for the analyses of thermal heating. In this paper the methods, which are applied for the structural layout of the ReFEx vehicle, are summarized and analysed. The introduced fast pre-analyses for the layout (chapter 2.1) deliver a first impression of the temperatures distribution of the vehicle. Nevertheless, it is clear that these temperatures are too high for both shown approaches, as expected. The usually following DLR development process applies in general the classical V-model of systems engineering to analyze a first design space and achieve possible solutions. This process is extended by developing a dataset based thermo-mechanic analysis (chapter 2.2).

This approach for the layout is compared to a fully coupled unsteady FSI simulation approach, based on DLR TAU calculations for CFD along the whole trajectory, considering the material properties through coupling using a high fidelity structural model (chapter 2.3). As expected, the file exchange based CFD/structure coupling of chapter 2.2 delivers more conservative results for the temperature distribution in most surface areas. Due to the reduced number of CFD simulations instead of a unsteady fully coupled simulation, the calculations time can be reduced in general for this chosen approach of structure layout. The time accurate fully coupled simulation along the trajectory delivers more precise temperatures. The peak differences of the predicted temperatures on the canards for example are predicted about $\Delta T = 79\,\mathrm{K}$ to $\Delta T = 413\,\mathrm{K}$ at the leading / trailing edges higher by the database exchange based CFD/structure coupling but compare well on the surface between. The main body of ReFEx is well captured in both methods differing at worst on the nose cone by 17% at the time point of peak heating at $t = 44\,\mathrm{s}$. The fin varies between 21 K to 121 K, depending on the selected flight phase.

The dataset based approach delivers intended higher temperatures to be on the safe side during the layout and design phase. To predict precise temperatures for the whole vehicle, time accurate full-coupled unsteady simulations are required and can be used for a final proof of temperature-sensitive components, like the wrap-up around GPS antenna.

References

[1] Ansys Inc. Ansys. https://www.ansys.com/de-de/.

[2] F. Barz and M. Franze. Comparison of different fidelity approaches for the coupled aerothermodynamic heating of hypersonic reentry vehicle. In *HiSST - 3nd International Conference on High-Speed Vehicle Science Technology*, 2024.

[3] W. Bauer et al. DLR reusability flight experiment refex. *Acta Astronaut.*, 168, 2019.

[4] J.A. Fay and F.R. Riddell. Theory of stagnation point heat transfer in dissociated air. *Journal of the aeronautical Sciences*, 25(2), 1958.

[5] Sanford Gordon, Bonnie J. Mcbride, and Bonnie J. Mcbride. Computer program for calculation of complex chemical equilibrium compositions and applications. Part 1: Analysis. Report NASA-RP-1311, NASA Lewis Research Center, Cleveland, Ohio, USA, October 1994.

[6] R. N. Gupta, J. M. Yos, and R. A. R. A. Thompson. P. Lee. A review of reaction rates and thermodynamic and transport properties for an 11-species air model for chemical and thermal nonequilibrium calculations to 30000 K. Technical Report 1232, NASA Reference Publication, 1990.

[7] Stefan Langer, Axel Schwöppe, and Norbert Kroll. The DLR Flow Solver TAU - Status and Recent Algorithmic Developments. In *52nd Aerospace Sciences Meeting*, National Harbor, Maryland, January 2014. American Institute of Aeronautics and Astronautics.

[8] A. Mack and V. Hannemann. Validation of the unstructured dlr-tau-code for hypersonic flows. In *32nd AIAA Fluid dynamics conference and exhibit*. AIAA Paper 2002-3111, 2002.

[9] Michael Meinel and Gunnar ´Olafur Einarsson. The FlowSimulator framework for massively parallel CFD applications. In *State of the Art in Scientific and Parallel Computing*, University of Iceland, Reykjavi, June 2010.

[10] C. Merrem, V. Wartemann, H. Elsäßer, T. Ruhe, and T. Eggers. Rolling capabilities of the experimental vehicle refex. In *HiSST - 2nd International Conference on High-Speed Vehicle Science Technology*, 2022.

[11] NOAA, NASA, and U.S. Air Force. U.S. Standard Atmopshere 1976. Report NASA-TM-X74335, NOAA, NASA, U.S. Air Force, Washington D.C., USA, 1976.

[12] Lars Reimer, Ralf Heinrich, Sven Geisbauer, Tobias Leicht, Stefan Görtz, Markus Raimund Ritter, and Andreas Krumbein. Virtual Aircraft Technology Integration Platform: Ingredients for Multidisciplinary Simulation and Virtual Flight Testing, January 2021.

[13] U. Reisch and T. Streit. Surface inclination and heat transfer methods for reacting hypersonic flow in thermochemical equilibrium. In *New Results in Numerical and Experimental Fluid Mechanics: Contributions to the 10th AG STAB/DGLR Symposium*, 1996.

[14] P. Rickmers, W. Bauer, S. Kottmeier, T. Delovski, B. Suhr, and S. Klinkner. Flight experiment – refex: Agile aiv processes for prototype flight experiments. In *73rd International Astronautical Congress (IAC)*. IAC-22-D2.6.4x68659, 2022.

[15] Andreas Schütte. *Wirbelumströmungen an gepfeilten Flügeln mit runden Vorderkanten*. DLR Forschungsbericht 2015-40, Dissertation, Technische Universität Braunschweig, Deutschland, 2015.

[16] D. Schwamborn, T. Gerhold, and R. Heinrich. The dlr tau-code: recent applications in research and industry. european conference on computational fluid dynamics. In *ECCOMAS CFD*, 2006.

[17] Philippe R. Spalart and Steven R. Allmaras. A One-Equatlon Turbulence Model for Aerodynamic Flows. In *30th Aerospace Sciences Meeting & Exhibit*, Reno, Nevada, USA, 1992.

[18] Yasuh Wada and Meng-Sing Liou. An Accurate and Robust Flux Splitting Scheme for Shock and Contact Discontinuities. 18(3):633–657, 1997.